Geophysical Journal International

Geophys. J. Int. (2015) **201,** 475–484 doi: 10.1093/gji/ggv036
GJI Geomagnetism, rock magnetism and palaeomagnetism

Magnetic properties of Archean gneisses from the northeastern North China Craton: the relationship between magnetism and metamorphic grade in the deep continental crust

Hongcai Wang,[1] Qingsheng Liu,[2] Weihua Zhao,[1] Zhiyong Li[2] and Jianping Zheng[3]

[1] *Institute of Geomechanics, Chinese Academy of Geological Sciences, Beijing* 100081*, P.R. China*
[2] *Department of Geophysics, China University of Geosciences, Wuhan* 430074*, P.R. China. E-mail: lqs321@cug.edu.cn*
[3] *Faculty of Earth Sciences, China University of Geosciences, Wuhan* 430074*, P.R. China*

Accepted 2015 January 19. Received 2015 January 17; in original form 2014 September 13

SUMMARY

Magnetic mineralogy of crustal rocks has important implications for understanding continental crustal evolution and origin of regional magnetic anomalies. However, magnetic properties of the deep continental crust are still poorly understood. In this paper, measurements of density (ρ), mass-specific magnetic susceptibility (χ), natural remanent magnetization (NRM) and magnetic hysteresis loops, temperature-dependent magnetic susceptibility (χ–T), chemical and mineral analyses were conducted on Archean gneiss samples from the Jixian petrophysical section in the Precambrian terrain, northeastern North China Craton, with the aim of refining understanding of magnetic phase transformations in the deep crustal rocks. Results show that density and rock magnetic properties change distinctly with metamorphic facies. The dominant magnetic mineral is magnetite, while a little hematite is present in a few samples. Together with geochemical and mineralogical compositions, it is inferred that progressive increase in metamorphic grade from east to west is the major cause for magnetic enhancement of the lower crust in the studied section. Therefore, we conclude that study of magnetic phases of deep crustal rocks can offer important insights into the history of high metamorphic grade terranes.

Key words: Magnetic mineralogy and petrology; Rock and mineral magnetism; Crustal structure.

1 INTRODUCTION

Sources of the geomagnetic field are located both within and external to the Earth. There is a natural dichotomy in the magnetic fields deriving from internal sources between those generated within the Earth's core and those originating in the crust and upper mantle (Kletetschka & Stout 1998; Langel & Hinze 1998; Pilkington & Percival 1999; Ravat *et al.* 2002). Deep seated rocks contain variable amounts of magnetic minerals, which commonly produce a magnetic field mappable at the Earth' surface (Arkani-Hamed & Srangway 1985; Schlinger 1985; Frost & Shive 1986; Schlinger *et al.* 1989; Piper *et al.* 2003; Brown & McEnroe 2008; Dunlop *et al.* 2010; Ferré *et al.* 2013, 2014; Liu *et al.* 2013). The determination of factors controlling the occurrence and abundance of mineral phases in deep crust is still in its infancy. Many geological processes in deep crust can generate a crustal magnetic field by rock magnetic variation, such as progressive metamorphism (Wasilewski & Fountain 1982; Schlinger 1985; Wasilewski & Warner 1988; Liu *et al.* 1994, 2000; Dunlop *et al.* 2010), retrogressive metamorphic effects (Liu *et al.* 2007, 2009; Xu *et al.* 2009), fractural crystallization (Liu *et al.* 2008, 2012), serpentinized processes (Toft *et al.* 1990; Oufi *et al.* 2002; Liu *et al.* 2010, 2015) and hydration processes (Toft *et al.* 1993). However, the balance between these processes, regional metamorphism and rock magnetic properties remain unclear.

The magnetic structure of deep crust controls the characteristics of regional middle–long wavelength magnetic anomalies (Liu *et al.* 2015). Archean rocks exposed on the surface recorded chemical composition and mineral assemblages in deep crust (Shive & Fountain 1988; Frost 1991; Dunlop *et al.* 2010; Brown *et al.* 2013; Liu *et al.* 2013). There are two important aspects to the study of magnetic mineral occurrence in crustal rocks. One concerns the factors that control Fe–Ti oxides, including the subsolidus reactions that affect the oxide during cooling of plutonic rocks (Banerjee 1991; Frost & Lindsley 1992; Lindsley & Frost 1992). Although they are nominally metamorphic reactions, they have been given little attention by metamorphic petrologists (and even less by igneous petrologists) and are poorly understood. The second concerns the reactions that control the occurrence and abundance of Fe–Ti oxides during metamorphism of rocks of various protoliths (Frost 1991; Frost & Lindsley 1992; Lindsley & Frost 1992; Doubrovine &

Tarduno 2004, 2006). Therefore, using high-grade metamorphic rocks (i.e. Archean gneiss) exposed on the surface to study magnetic structure of the deep crust have important implications for understanding the evolution of the deep crust (Shive *et al.* 1992).

The Jixian petrophysical section located in Precambrian terrain of the northeastern North China Craton dominantly consists of high amphibolite facies and granulite facies rocks from the eastern to the western sectors. In this paper, we investigate the magnetic properties of 47 samples, and mineral assemblages and chemical compositions of representative samples. Our main objective is to elucidate the relationships between rock magnetism and metamorphic grade in the deep continental crust.

2 GEOLOGICAL BACKGROUND AND SAMPLING

The Jixian petrophysical section is regarded as a typical example of a section of the lower continental crust. The section exposes early Precambrian metamorphic basement in the northeastern North China Craton (Zhang & Cong 1982; Zhang & Piper 1994; Deng *et al.* 1999; Piper & Zhang 1999, 2011; Fig. 1). The section studied is from the Qinghuandao in east by Qinglong, Qianan, Kuancheng, Qianxi, Zunhua, Jixian to Miyun in Beijing city, and whole section is *ca.* 220 km long (Fig. 1). Rocks mainly consist of Archean gneiss (Ar) with little amphibolite, granite and early Palaeozoic rocks. Taken the lithologic differences into consideration, two to three samples were collected at each sampling site, and 47 samples were obtained in total from 26 sites (No. 4–31, Fig. 1 and Table 1). The section has been divided into three segments: the eastern segment including samples No. 5–25, the middle segment: No. 26–47, and the western segment: from No. 48 to 54 (Table 1).

3 ANALYTICAL METHODS

3.1 Density and magnetic measurements

Density (ρ) was measured using a LP-1002 gravity densimeter, with a resolution of 0.01 ($\times 10^3$) kg m^{-3} and a corresponding precision of 0.03 per cent. Mass-specific magnetic susceptibility (χ) and natural remanent magnetization (NRM) of all samples were determined using Kappabridge KLY-3S magnetic susceptibility meter (AGICO, Inc.), and DSM-2 and SSM-2A Spinner Magnetometers (Schonsted Company, USA), respectively. The Köenigasberger ratio (Q) is given by NRM/J_i, where J_i is the induced magnetization ($=\chi \times H$, where H is the intensity of the local geomagnetic field and $H = 0.06$ mT).

Magnetic hysteresis loops were measured on powdered samples using a MicroMag$^{\mathrm{TM}}$ Model 3900 vibrating sample magnetometer (VSM, Princeton Measurements Corp.); the maximum applied field was 1.0 T. Hysteresis parameters, saturation magnetization

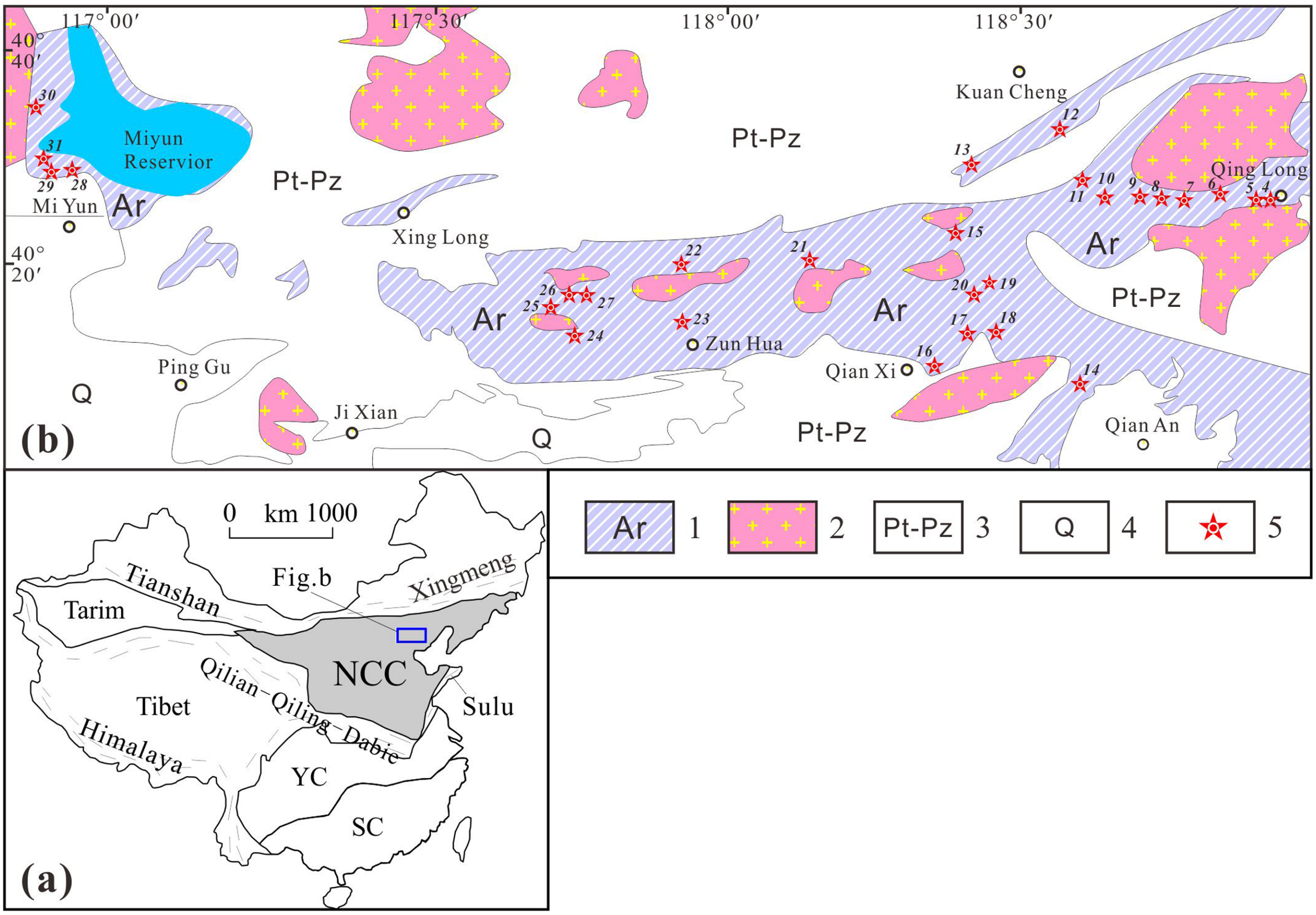

Figure 1. Geological map of the study area and sampling sites. NCC, North China Craton; YC, Yangtze Craton; SC, South Cathysia. East segment: No. 5–No. 14; Middle segment: No. 15–No. 27; West segment: No. 28–No. 31. 1. Archean gneiss; 2. Granite; 3. Pt-Pz, Proterozoic-Paleozoic; 4. Q, Quaternary; 5. Sampling site.

Table 1. Density and magnetic parameters of Archean gneiss terrain rocks from the northeastern North China Craton.

Sample	Site	ρ	χ	NRM	J_i	Q	χ_{ferri}	M_s	M_{rs}	B_c	B_{cr}	M_{rs}/M_s	B_{cr}/B_c	M_{rs}/χ
Eastern segment (20)														
5	4-Qinglong	2.69	0.10	0.01	0.00	1.51	0.00	0.81	0.12	11.49	70.57	0.15	6.14	1.19
6		2.69	0.08	0.00	0.00	0.94	0.01	0.67	0.10	22.57	75.86	0.15	3.36	1.30
7	5	2.68	10.57	2.45	0.46	5.37	12.40	625	37.50	3.38	15.38	0.06	4.55	3.55
8		2.65	1.40	0.40	0.06	6.69	1.13	127	9.98	8.78	37.43	0.08	4.26	7.14
9	6	2.65	0.10	0.02	0.00	4.63	0.14	2.10	0.05	1.89	51.49	0.02	27.31	0.49
10		2.65	0.36	0.22	0.02	14.24	0.14	8.43	2.48	46.84	103.76	0.29	2.22	6.95
11		2.66	0.25	0.21	0.01	19.54	0.41	36.3	3.39	8.77	41.06	0.09	4.68	13.40
12	7	2.64	1.91	0.13	0.08	1.60	7.17	725	34.6	5.94	36.92	0.05	6.22	18.12
13		2.68	0.88	0.13	0.04	3.34	2.73	216	13.30	6.12	55.23	0.06	9.02	15.18
14	8	2.75	0.21	0.01	0.01	1.09	0.11	3.44	0.34	11.00	83.15	0.10	7.56	1.65
15		2.79	0.73	0.11	0.03	3.59	3.71	228	14.50	4.41	23.80	0.06	5.40	19.86
16	9	2.91	11.99	2.87	0.52	5.54	11.90	1160	25.60	2.89	16.29	0.02	5.63	2.14
17		2.76	0.10	0.01	0.00	2.21	0.20	3.09	0.40	10.12	29.46	0.13	2.91	3.93
18	10	2.81	1.89	0.11	0.08	1.34	0.06	25.3	0.40	1.19	16.41	0.02	13.75	0.21
19		2.90	34.47	6.82	1.49	4.58	39.30	3600	44.40	1.38	16.42	0.01	11.90	1.29
21	12-Kuancheng	2.56	0.20	0.13	0.01	15.00	0.12	9.19	0.71	5.65	32.51	0.08	5.76	3.47
22		2.75	0.31	0.05	0.01	3.47	0.22	7.24	0.59	4.78	31.41	0.08	6.58	1.88
23		2.68	1.17	0.10	0.05	2.07	4.47	504	21.50	5.85	38.82	0.04	6.64	18.45
24	13-Kuancheng	2.65	0.33	0.07	0.01	4.64	0.11	17.40	0.32	1.70	19.86	0.02	11.69	0.97
25	14-Qian'an	2.55	0.06	0.03	0.00	8.67	1.22	7.76	1.77	13.99	51.64	0.20	3.69	28.55
	Mean	2.71	3.36	0.69	0.15	5.50	4.28	365.34	10.60	8.94	42.37	0.09	7.46	7.49
	σ	0.09	8.05	1.65			9.09	824.74	14.42					
Middle segment (20)														
26	15	2.84	6.72	0.59	0.29	2.02	18.80	1270	23.80	1.52	14.77	0.02	9.69	3.54
27		2.83	6.96	2.19	0.30	7.29	0.30	68.9	5.56	9.83	47.67	0.08	4.85	0.80
29	16-Qianxi	2.89	2.67	2.71	0.12	23.49	2.18	192	25.20	11.95	35.09	0.14	2.94	9.34
30	17	3.07	0.69	1.08	0.03	36.41	0.53	41.4	6.11	15.99	56.20	0.15	3.52	8.89
31		3.07	0.68	1.06	0.03	36.00	0.44	43.4	3.40	7.87	32.70	0.08	4.15	4.97
32	18	2.65	2.58	1.10	0.11	9.84	0.43	33.3	0.78	2.22	18.01	0.02	8.11	0.30
34	20	2.73	4.35	0.51	0.19	2.70	2.30	609	20.60	3.40	19.38	0.03	5.71	4.74
35		2.81	6.43	0.86	0.28	3.11	7.20	853	54.10	5.18	17.63	0.06	3.40	8.41
36	21-Zunhua	2.70	4.72	0.34	0.20	1.68	12.10	2400	5.34	0.22	12.24	0.00	56.43	1.13
37	22	2.65	15.99	1.71	0.69	2.47	30.50	1320	24.00	1.64	13.22	0.02	8.05	1.50
38		2.70	5.90	0.50	0.26	1.95	17.00	383	4.31	1.35	17.69	0.01	13.14	0.73
39	23	2.64	0.21	0.03	0.10	3.10	3.85	2.4	0.52	15.34	81.98	0.21	5.34	2.50
40	24	2.76	4.55	0.47	0.20	2.37	0.01	614	90.60	19.64	61.47	0.15	3.13	19.93
41		2.77	4.10	0.26	0.18	1.48	5.53	835	136	21.46	59.80	0.16	2.79	33.21
42	25	2.79	7.67	0.76	0.33	2.30	7.53	1120	31.80	2.55	21.72	0.03	8.51	4.15
43		2.73	2.66	0.38	0.12	3.28	15.40	537	21.00	3.40	16.67	0.04	4.90	7.90
44	26	2.67	0.04	0.01	0.00	5.23	7.45	1.56	0.16	3.15	37.02	0.10	11.74	3.55
45		2.79	0.04	0.03	0.00	13.94	0.01	10.3	0.31	2.82	25.07	0.03	8.88	7.21
46	27	2.64	0.03	0.03	0.00	20.43	0.09	0.81	0.17	2.66	38.77	0.21	14.59	5.41
47		2.66	2.61	0.53	0.11	4.72	0.000	1620	118	7.76	54.49	0.07	7.03	45.23
	Mean	2.77	3.98	0.76	0.17	9.19	6.59	597.75	28.59	7.00	34.08	0.08	9.35	8.67
	σ	0.13	3.80	0.73			8.30	668.94	40.39					
Western segment (7)														
48	28-Miyun	2.76	6.55	0.28	0.28	0.98	18.30	4010	177	4.91	23.56	0.04	4.80	27.01
49		3.15	19.62	1.67	0.85	1.98	43.40	1510	128	10.57	38.36	0.08	3.63	6.52
50	29	2.75	22.35	1.57	0.97	1.63	14.40	2070	64.70	2.98	15.55	0.03	5.22	2.89
51		2.79	22.42	20.26	0.97	20.93	26.30	730	28.40	3.82	17.39	0.04	4.56	1.27
52	30	2.76	0.26	0.04	0.01	3.70	8.89	36.7	3.22	11.77	72.91	0.09	6.20	12.63
53		2.70	0.20	0.15	0.01	11.57	0.24	19.2	2.01	13.84	71.40	0.10	5.16	6.74
54	31	2.72	13.11	1.41	0.57	2.49	0.07	1720	9.93	0.82	22.48	0.01	27.41	0.76
Mean		2.80	12.09	3.63	0.52	6.18	15.94	1442.27	59.04	6.96	37.38	0.06	8.14	8.26
σ		0.16	9.83	7.37			15.37	1389.07	68.82					

Notes: ρ, density (10^3 kg m^{-3}); χ, mass susceptibility (10^{-6} m^3 kg^{-1}); NRM, natural remanent magnetization (10^{-3} Am^2 kg^{-1}); J_i, induced magnetization ($=\chi \times H$, H is local geomagnetic field) (10^{-3} Am^2 kg^{-1}); Q, Köenigsberger ratio (NRM/J_i); χ_{ferri} is ferrimagnetic susceptibility calculated from magnetic hysteresis (10^{-6} m^3 kg^{-1}); M_s, saturation magnetization (10^{-3} Am^2 kg^{-1}); M_{rs}, saturation isothermal remanent magnetization (10^{-3}Am^2 kg^{-1}); B_c, intrinsic coercivity (mT); B_{cr}, remanent coercivity (mT), and M_{rs}/χ (10^3 Am^{-1}). ρ, χ and NRM are from solid samples, magnetic hysteresis parameters are from powder samples. σ, standard deviation.

(M_s), saturation remanence (M_{rs}) and coercive force (B_c) were calculated after para-/diamagnetic correction. Remanence coercivity (B_{cr}) was determined by backfield measurements after reaching 1.0 T. The ferrimagnetic susceptibility (χ_{ferri}) is calculated from bulk magnetic susceptibility (χ) subtracting χ_{para} ($\chi_{\text{ferri}} = \chi - \chi_{\text{para}}$, χ_{para} is paramagnetic susceptibility). The temperature dependence of χ was conducted from room temperature to ∼700 °C in an Argon environment with steps of 5 °C using a Kappabridge KLY-3S magnetic susceptibility meter equipped with a CS-2 furnace.

3.2 Chemical and mineralogical analyses

Based on the magnetic measurements, representative samples were chosen for optical microscopy and chemical composition analyses. Polished thin sections of the specimens were examined under both transmitted and reflected light to identify the mineralogical components. In particular, these observations are used to identify the metamorphic facies, the major mineral assemblage for samples with different metamorphic degree. Whole-rock major elements of all samples were determined by XRF06 in the ALS Global, Guangzhou, China.

4 RESULTS

4.1 Petrology, geochemistry and mineral assemblage

Samples are dominantly various gneisses of granulite facies grade, sometimes showing degrees of retrogression and including felsic gneiss, feldspar granulite, amphibole–two pyroxene granulite, garnet-bearing felsic granulite (Fig. 2). The whole-rock chemical composition and major mineral assemblages for representative samples are shown in Tables 2 and 3. The concentrations of SiO_2 vary from 43.70 to 67.31 per cent, and are attributed to primary acidic, intermediate and basic igneous compositions. SiO_2 concentrations of samples from the middle and western segments generally are lower than those in the eastern segment. Total Fe contents are between 2.73 and 16.78 per cent for representative samples, and the Fe contents of samples in the middle and western segments (5.11–16.78 per cent) are generally higher than those in the eastern segment (Table 2).

Microphotographs of representative samples are illustrated in Fig. 2. On the basis of mineral assemblages, from the eastern segment to the western segment, metamorphic facies of samples vary

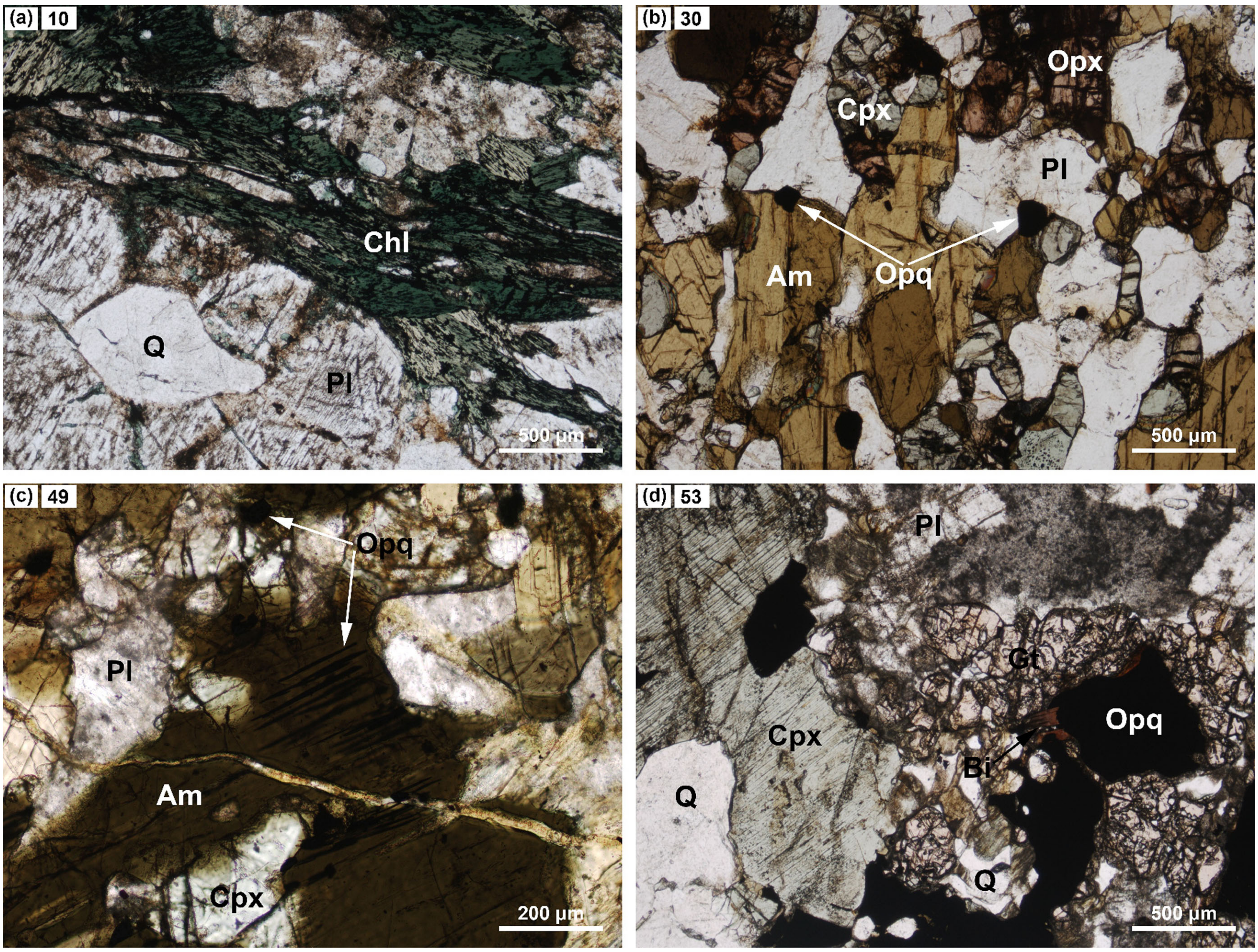

Figure 2. Microphotographs of representative samples. (a) Felsic leptynite from the eastern segment, containing Pl + Chl + Q; (b) Amphibole two-pyroxene granulite from the middle segment, containing Am + Cpx + Opx + Pl + Opq; (c) and (d) Grt-pyroxene amphibolite and Gt-bearing felsic granulite from the western segment, containing Am + Cpx + Pl + Opq and Gt + Cpx + Pl + Bi+ Q + Opq, respectively. Am, amphibole; Bi, biotite; Chl, chlorite; Cpx, clinopyroxene; Gt, garnet; Opq, opaque mineral; Opx, orthopyroxene; Pl, plagioclase; Q, quartz.

Table 2. Geochemical composition of representative samples (wt%).

Sample	Rock type	SiO_2	TiO_2	Al_2O_3	FeO_T	Cr_2O_3	MnO	MgO	CaO	Na_2O	K_2O	P_2O_5	SrO	BaO	LOI	Total
	Eastern segment															
7	Granodiorite gneiss	64.67	0.49	16.33	4.49	<0.01	0.06	1.81	3.53	4.51	3.06	0.28	0.1	0.11	0.52	99.96
10	Felsic leptynite	67.31	0.27	15.66	2.73	<0.01	0.05	1.02	2.67	3.44	3.54	0.08	0.02	0.06	3.07	99.93
13	Granite gneiss	64.54	0.42	15.61	4.15	<0.01	0.06	1.96	1.76	5.13	3.29	0.21	0.07	0.13	2.64	99.96
16	Felsic mylonite	43.70	3.46	13.22	16.62	0.01	0.13	4.89	6.60	2.13	1.63	1.66	0.03	0.13	5.46	99.67
18	Garnet-Bi-bearing leptynite	59.90	0.47	13.35	9.79	0.01	0.14	4.02	4.99	3.44	0.90	0.10	0.05	0.03	2.01	99.20
19	Felsic mylonite	55.62	1.20	17.31	8.98	<0.01	0.08	2.59	4.61	3.88	3.33	0.75	0.08	0.14	1.24	99.81
23	Felsic gneiss	60.20	0.65	14.76	6.67	0.03	0.06	3.76	2.51	3.53	2.78	0.27	0.03	0.12	4.48	99.86
25	Granulite	53.38	0.93	16.81	8.30	0.03	0.11	5.06	8.34	4.34	0.87	0.39	0.08	0.04	0.94	99.62
	Middle segment															
26	Amphibole Two-pyroxene granulite	56.94	0.69	16.59	7.90	0.01	0.11	4.02	7.13	4.5	0.69	0.21	0.08	0.04	0.91	99.83
29	Amphibole Two-pyroxene granulite	52.79	0.62	15.96	10.32	0.01	0.16	5.6	9.18	3.76	0.71	0.11	0.03	0.07	0.57	99.89
30	Amphibole Two-pyroxene granulite	49.88	0.83	14.74	12.41	0.04	0.17	7.29	9.97	2.86	0.8	0.06	0.02	0.01	0.87	99.96
31	Amphibole Two-pyroxene granulite	48.95	0.83	14.59	12.94	0.04	0.2	8.07	10.12	2.65	0.85	0.06	0.02	0.02	0.4	99.73
35	Felsic granulite	57.55	0.57	14.92	8.21	0.02	0.11	4.67	6.06	4.00	1.38	0.16	0.07	0.05	2.11	99.89
37	Felsic granulite	62.05	0.43	15.06	6.73	0.02	0.08	3.19	3.03	3.30	3.99	0.31	0.08	0.17	1.16	99.60
42	Bi-Pl gneiss	60.86	0.64	15.87	7.75	0.01	0.08	3.12	3.26	3.19	2.41	0.14	0.04	0.07	1.55	98.99
47	Felsic leptynite	64.58	0.28	14.55	6.01	<0.01	0.04	2.40	3.37	3.65	1.82	0.03	0.05	0.08	2.92	99.78
	Western segment															
49	Gt-pyroxene amphibolite	45.48	1.26	12.6	16.78	0.08	0.27	8.22	9.31	2.59	1.16	0.28	0.05	0.03	1.84	99.94
53	Gt-felsic granulite	62.79	0.70	16.38	5.11	<0.01	0.08	2.17	3.91	4.25	3.13	0.28	0.09	0.15	0.81	99.85
54	Bi-Pl gneiss	57.99	0.60	17.62	5.67	<0.01	0.07	2.49	3.61	4.79	5.12	0.39	0.11	0.15	1.12	99.73

Note: FeO_T, total Fe content.

Table 3. Mineral assemblage of representative samples.

Site	No.	Rock type	Am	Bi	Q	Gt	K-Feldspar	Opx	Cpx	Pl	Cal	Act	Chl	Epi	Opq
Qinglong	7	Granodiorite gneiss	18	7	35		20			20					
Qinglong	10	Felsic leptynite			15		40			10			25		2
Qinglong	13	Granite gneiss			20–25					65		15			
Qinglong	16	Felsic mylonite		20						40–50			25		10
Qinglong	18	Garnet-Bi-bearing leptynite		20	15	10				50					
Qinglong	19	Felsic mylonite	3	15	30					35–40	7		2	3	
Kuancheng	23	Felsic gneiss		5–10	30		45				5		10–15		
Kuancheng	25	Granulite	35		15			5	2	40					3
Kuancheng	26	Amphibole Two-pyroxene granulite	20		5			10	15	45					5
Qianxi	29	Amphibole Two-pyroxene granulite	20		10			10–15	10–15	45					
Qianxi	30	Amphibole Two-pyroxene granulite	40		5–10			20–25	15	15					
Qianxi	31	Amphibole Two-pyroxene granulite	40		5–10			15	20–25	15					
Qianxi	35	Felsic granulite			10		45	13	15	10					4
Zunhua	37	Felsic granulite		15	20		50	8		7					
Zunhua	42	Bi-Pl gneiss		25–30	15–20		10			30–35		10			
Zunhua	47	Felsic leptynite			20–25		35	28					10–15		2
Miyun	49	Gt-pyroxene amphibolite	50			10			30	5					5
Miyun	53	Gt-felsic granulite	3	2	5	10	30	5–10	15	30					5
Miyun	54	Bi-Pl gneiss		25	10		10			45–50		5–10			

Note: Act, actinolite; Am, amphibole; Bi, biotite; Cal, calcite; Chl, chlorite; Cpx, clinopyoxene; Epi, epidote; Gt, garnet; Opq, opaque mineral; Opx, orthopyroxene; Pl, plagioclase; Q, quartz.

from high-amphibolite facies to granulite facies. The major mineral assemblages comprise the following (Fig. 2 and Table 3):

$$\begin{aligned}
\text{Eastern segment}: \quad & \text{amphibole} + \text{plagioclase} + \text{quartz} \\
& + \text{biotite} + \text{chlorite} + \text{opaque} \\
\text{Middle segment}: \quad & \text{amphibole} + \text{clinopyroxene} + \text{orthopyroxene} \\
& + \text{plagioclase} + \text{biotite} + \text{quartz} + \text{opaque} \\
& + \text{K-feldspar} \\
\text{Western segment}: \quad & \text{amphibole} + \text{quartz} + \text{clinopyroxene} \\
& + \text{orthopyroxene} + \text{plagioclase} + \text{opaque} \\
& + \text{biotite} + \text{K-feldspar}
\end{aligned}$$

4.2 Density and magnetic properties

4.2.1 Density and general magnetic properties

Densities and magnetic parameters of 47 samples are summarized in Table 1. Average values of ρ are 2.71 ± 0.09, 2.77 ± 0.13 and 2.80 ± 0.16 ($\times 10^3$) kg m^{-3} for the eastern, middle and western segments, respectively (Table 1). From the eastern, middle to western segments, average values of χ and NRM are 3.36 ± 8.05, 3.98 ± 3.80, 12.09 ± 9.83 ($\times 10^{-6}$) m^3 kg^{-1}; 0.69 ± 1.65, 0.76 ± 0.73, 3.63 ± 7.37 ($\times 10^{-3}$) Am^2 kg^{-1}, respectively (Table 1). These indicate that density and magnetic properties of rocks for the Jixian petrophysical section increase systematically from the eastern to the western segments (Figs 3a–c). Overall the Q values of the rocks

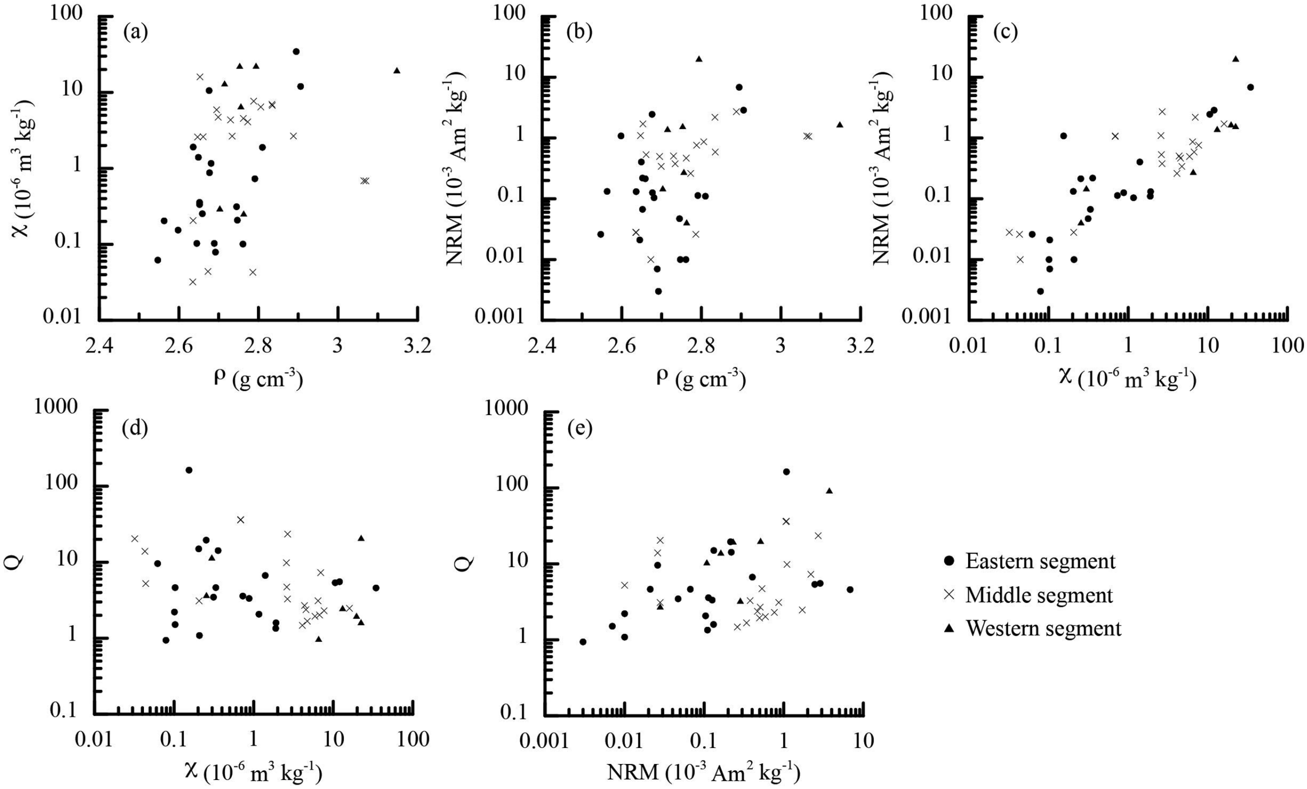

Figure 3. Scattergrams of different parameters for samples studied.

are higher than 1 (only two sample <1), and Q values of the rocks from the middle and western segments are higher than those from the eastern segment (Table 1). This indicates that the total magnetization of samples studied is mainly controlled by NRM more than by the induced magnetization (Figs 3d and e).

4.2.2 Magnetic hysteresis

Magnetic hysteresis parameters of all samples are listed in Table 1. From the eastern segment, the middle segment to the western segment, average values of M_s, M_{rs} and χ_{ferri} are 365.34 ± 824.74, 597.75 ± 668.94, 1442.27 ± 1389.07 ($\times 10^{-3}$) Am^2 kg^{-1}; 10.60 ± 14.42, 28.59 ± 40.39, 59.04 ± 68.82 ($\times 10^{-3}$) Am^2 kg^{-1} and 4.28 ± 9.09, 6.59 ± 8.30 to 15.94 ± 15.37 ($\times 10^{-6}$) m^3 kg^{-1}, respectively (Table 1). They indicate that average values of M_s, M_{rs}, χ_{ferri} increase systematically from east to west in parallel with the properties of χ and NRM (Table 1).

Magnetic hysteresis loops for representative samples are shown in Fig. 4. Samples from the eastern segment show a presence of dominant paramagnetic components (larger slope in high field) (No. 10, 18 and 23 in Fig. 4). Most of samples in the middle and western segments are a mixture of ferrimagnetic and paramagnetic components (No. 29, 35, 47 for the middle segment and 49, 53, 54 for the western segment in Fig. 4). In plot of M_{rs}/χ and B_{cr}, the most samples form a close cluster in the (titano)magnetite area (Peters & Dekkers 2003) (Fig. 5). The ratios of M_{rs}/M_s and B_{cr}/B_c for most samples plotted in the Day diagram occupy the pseudo-single-domain (PSD) region (Fig. 6; Dunlop 2002).

4.2.3 Temperature-dependent low-field magnetic susceptibility

Most samples have a single Curie temperature of $T_c = 580$ °C, corresponding to pure magnetite, which is independent of the type of rocks (Fig. 7). The cooling curves generally are higher than heating curves, which indicates that new magnetite formed at >600 °C, possibly by the transformation of Fe-bearing silicate minerals or non-stoichiometric magnetite in primary samples (Fig. 7; Tarling 1983; Dunlop *et al.* 2006; Liu *et al.* 2009, 2010, 2013). In addition, a hump somewhere between 250 and 350 °C in some samples probably displays the characteristic of maghemite inversion, or titanomaghemite (Fig. 7; Doubrovine & Tarduno 2004, 2006).

5 DISCUSSION

5.1 Magnetic mineralogy of the lower crust

Based on these experimental data, we propose that magnetic properties of rocks from the studied crustal section are predominantly due to the effect of magnetite (Figs 5 and 7). Close relations between χ versus NRM indicate uniform origin of magnetic minerals, and this is consistent with the probable PSD properties of magnetic minerals in most samples (Figs 3c and 6). These results are similar with that of continental lower crustal rocks from previously published studied (Schlinger 1985; Williams *et al.* 1985; Frost & Shive 1986; Wasilewski & Warner 1988; Liu *et al.* 1994, 2000; McEnroe *et al.* 2004; Dunlop *et al.* 2010; Liu *et al.* 2013). Samples in the eastern segment lack orthopyroxene and clinopyroxene, which indicates that the metamorphic grade of the eastern segment is clearly lower than those of the middle and western segments (Table 3 and Fig. 2). Therefore, we infer that the progressive exposure of deeper metamorphic rocks from east to west parallels the magnetic enhancement of rocks by regional metamorphism (Frost & Shive 1986; Shive & Fountain 1988; Shive *et al.* 1992; Liu *et al.* 2013).

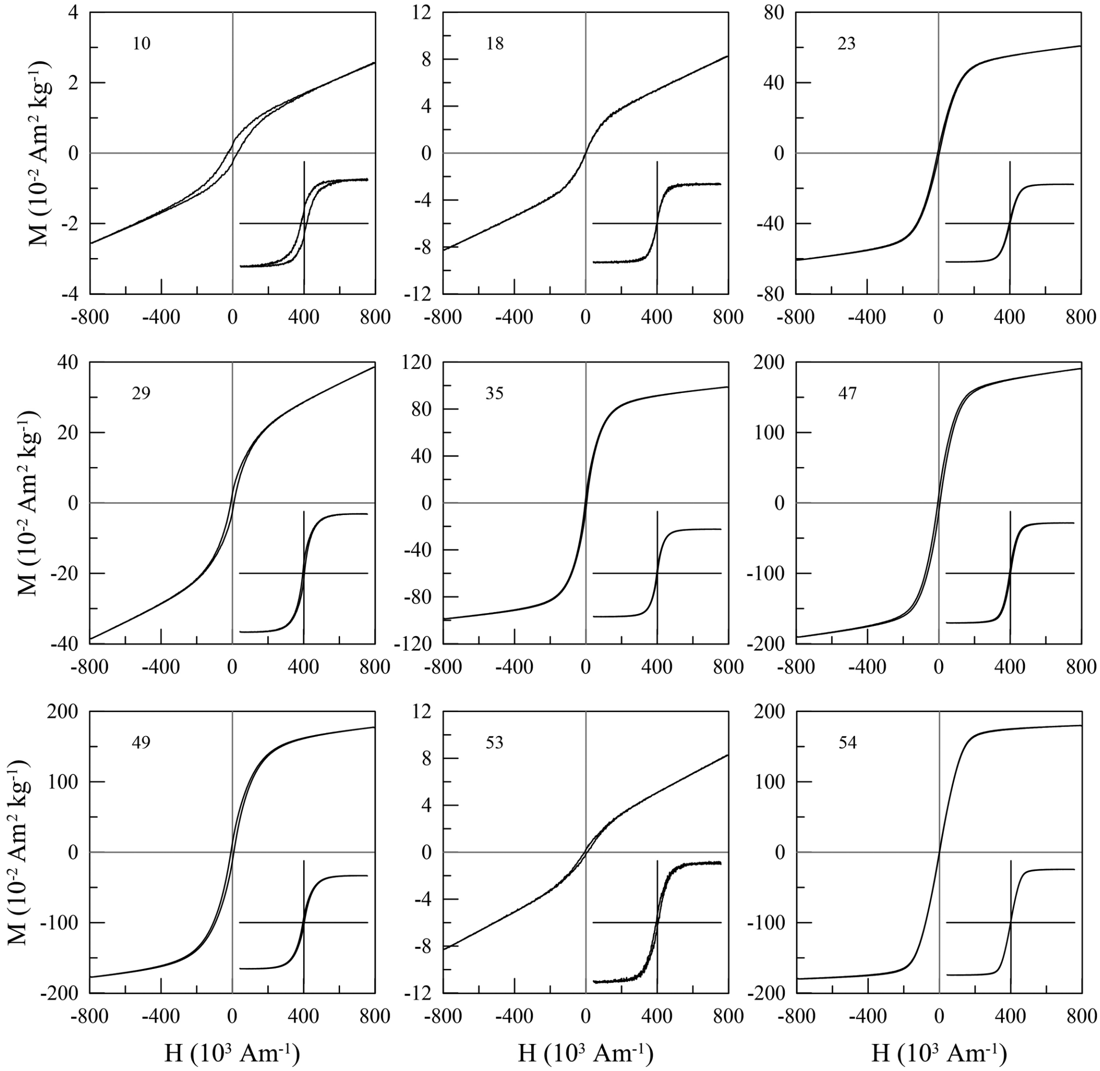

Figure 4. Magnetic hysteresis loops of representative samples. Maximum applied field is 1.0 T. No. 10, 18, 23 in the eastern segment, No. 29, 35, 47 in the middle segment, and No. 49, 53, 54 in the western segment. The insets are hysteresis loops after paramagnetic adjustment.

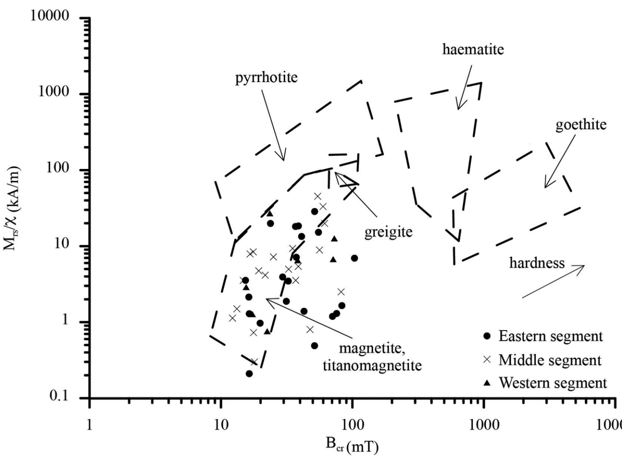

Figure 5. Plot of M_{rs}/χ versus B_{cr} (Peters & Dekkers 2003).

5.2 Magnetization of the lower crust

From east to west, the average values of ρ, χ and NRM increase systemically with increasing metamorphic degree from 2.68 to 2.80 ($\times 10^3$) kg m^{-3}, 3.36 to 12.09 $\times$ 10^{-6} m^3 kg^{-1} and 0.69 to 3.63 $\times$ 10^{-3} Am^2 kg^{-1} (Table 1), respectively. Magnetic properties of granulite facies rocks compare well with those of the lower continental crust in other sites, where χ, NRM and Q values of basic rocks generally are higher than 10^{-6} m^3 kg^{-1}, 10^{-4} Am^2 kg^{-1} and 1, respectively (Schlinger 1985; Wasilewski & Warner 1988; Belluso *et al.* 1990; Liu *et al.* 1994, 2013; Zhang *et al.* 1999; Dunlop *et al.* 2010; Liu 2011).

Magnetic properties of granulite facies rocks from the western segment in the Jixian petrophysical section compare well with those of the lower crustal rocks from the northern North China Craton. Volume susceptibility (κ), M_s and M_{rs} of granulite facies rocks from the Huai'an terrain are 4122 $\times$ 10^{-6} SI, 523.1 A m^{-1} and 74.9 A m^{-1} (Liu *et al.* 2013), and M_s and M_{rs} of Jining Group are 1068 and 138.4 A m^{-1} (Liu *et al.* 2000), respectively. κ values of basic and felsic granulites from the Datong–Huai'an Precambrian terrain are 1080–5634 $\times$ 10^{-6} SI and 1242–2475 $\times$ 10^{-6} SI, respectively (Zhang *et al.* 1999). The average κ value (33 844 $\times$ 10^{-6} SI) is considerably higher than that in Huai'an granulite facies rocks and felsic granulites, but is similar to basic granulites from the Datong–Huai'an Precambrian terrain (Zhang *et al.* 1999). M_s and M_{rs} values of our samples (average of 4038 and 165 A m^{-1}) are generally

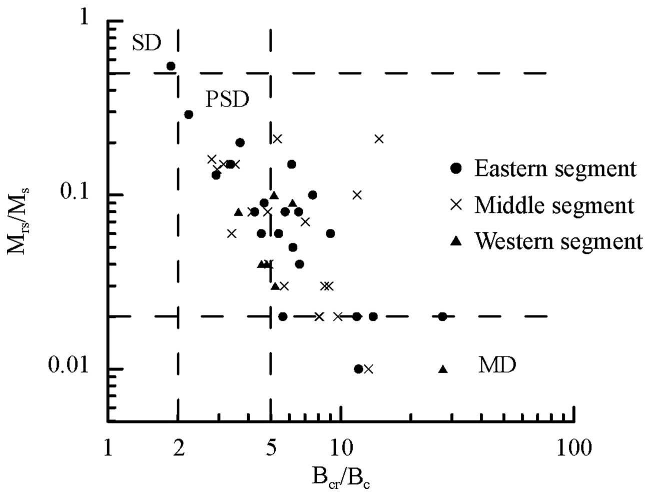

Figure 6. Day plot for representative samples (Dunlop 2002).

higher than those observed in the Jining Group and Huai'an terrain. Therefore, this finding indicates that magnetic properties of granulite facies rocks of the Jixian petrophysical section from the northeastern North China Craton are representative of magnetic properties of the Archean lower crust in the northern North China Craton.

5.3 Implications for metamorphic grade of the continental lower crust

The relationships between magnetic properties of crustal rocks and metamorphic facies are still poorly understood. In this metamorphic terrain, we are dealing with SiO_2 concentrations of ∼57.3 per cent, which is close to the granulite facies rocks in the Manjinggou–Wayaokou (MJG–WYK) section, northern North China Craton (Liu *et al.* 2013). Previous studies have shown that the transition from greenschist facies of upper crust to amphibolite facies of the middle crust, and to granulite facies of the lower crust, run in parallel with an increase in χ and NRM values (e.g. Wasilewski & Fountain 1982; Schlinger 1985; Ramachandran 1990; Olesen *et al.* 1991; Liu *et al.* 1994). Average values of χ and NRM from the western segment are 3.04, 3.60 times and 4.78, 5.26 times of the middle and eastern segments, respectively (Table 1), which clearly shows that magnetic properties in these three segments are controlled by metamorphic grade as found in other Precambrian shields (Wasilewski & Mayhew 1982; Schlinger 1985; Ramachandran 1990; Shive *et al.* 1992; Liu *et al.* 1994, 2000, 2013; Renne

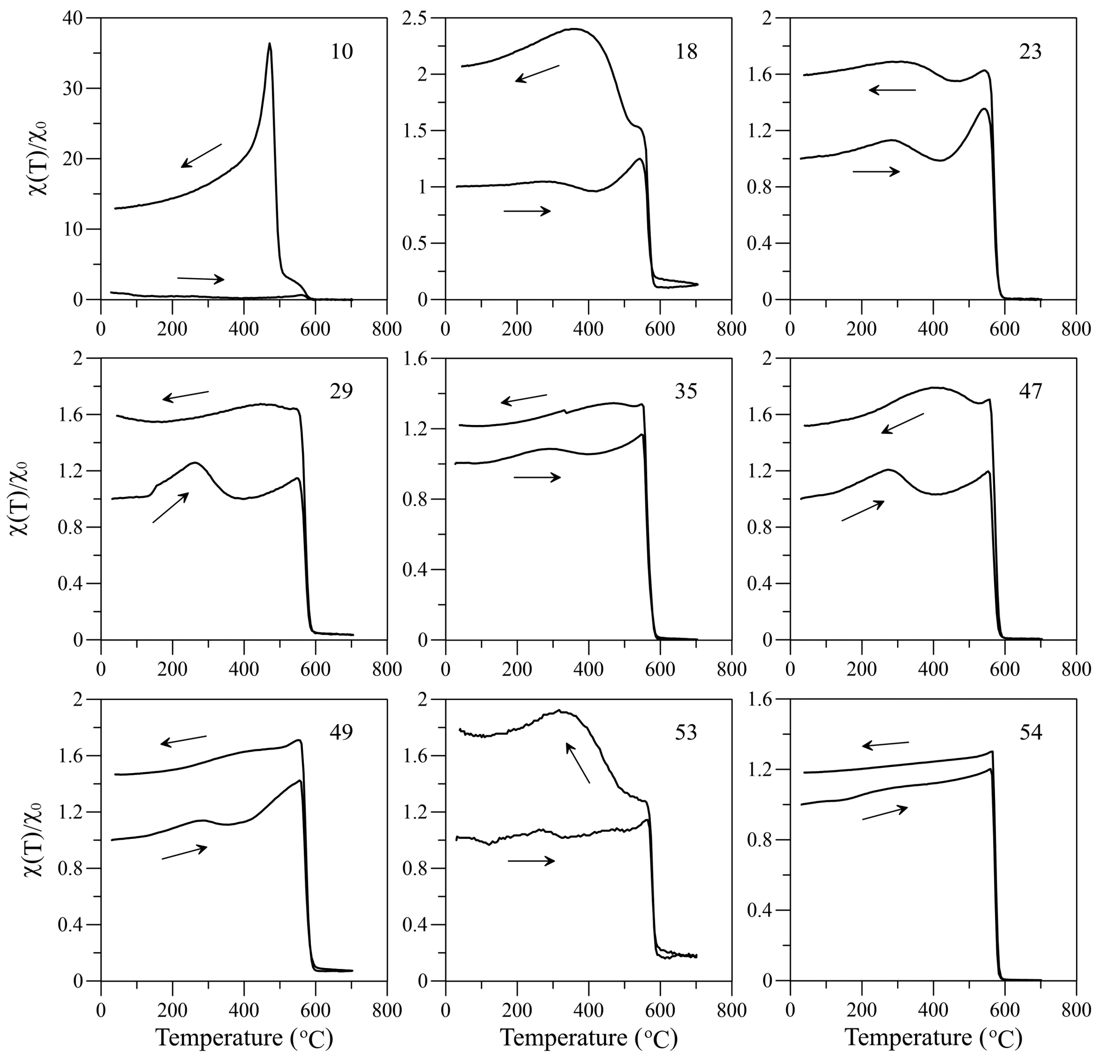

Figure 7. Temperature-dependent magnetic susceptibility curves for representative samples. Arrows indicate the heating and cooling processes.

et al. 2002; Piper *et al.* 2003). It is evident that prograde metamorphic transformation of amphibolite facies assemblage to granulite facies involves the formation of Fe–Ti oxide phases (e.g. ferrimagnetic magnetite, maghemite and titanomagnetite), whereas the retrograde metamorphism of intermediate–mafic granulites leads to the formation of relatively non-magnetic mineral assemblages.

6 CONCLUSIONS

Magnetic parameters, mineral assemblages and chemical composition of rocks from the Jixian petrophysical section located in the Precambrian terrain (northeastern North China Craton) indicate that ρ, χ and NRM of rocks are elevated systemically with increasing metamorphic grade from the eastern segment to the western segment. Magnetic mineralogy in granulitic lower crust from the Jixian petrophysical section is dominated by pseudo-single-domain magnetite. The magnetic properties of the Jixian petrophysical crustal rocks compare well with those resolved from studies of the Archean lower crust in the northern North China Craton (e.g. the Jining Group and Huai'an granulite terrain) in showing a comparable relationship between magnetic properties and metamorphic grade. Hence, the integrated study of rock magnetic and mineralogical properties can give insights into the metamorphic signatures of crustal basement derived from remote observation of magnetic anomalies. The combined interpretation of magnetic anomalies and rock magnetic properties is key to understand the structure and dynamics of deep continental crust.

ACKNOWLEDGEMENTS

Magnetic measurements were performed at the Key Laboratory of Seismic Observation and Geophysical Imaging, Institute of Geophysics, China Earthquake Administration. Mineralogical analyses were completed at the State Key Laboratory of Geological Processes and Mineral Resources in China University of Geosciences (Wuhan). This study was supported by the National Natural Science Foundation of China (Nos 41374094, 91214204 and 41130315) and the Chinese Geological Survey Project (Grant No. 2014-01-034-004).

REFERENCES

Arkani-Hamed, J. & Srangway, D.W., 1985. Lateral variations of apparent susceptibility of lithosphere deduced from Magasat dada, *J. geophys. Res.,* **90,** 2655–2664.

Banerjee, S.K., 1991. Magnetic properties of Fe-Ti oxides, *Rev. Miner.,* **25,** 107–128.

Belluso, E., Giuseppe, B. & Roberto, L., 1990. New data on the rock magnetism in the Ivrea-Verbano Zone (Northern Italy) and its relationship to the magnetic anomalies, *Tectonophysics,* **182,** 79–89.

Brown, L.L. & McEnroe, S.A., 2008. Magnetic properties of anorthosites: a forgotten source for planetary magnetic anomalies?, *Geophys. Res. Lett.,* **35,** L02305, doi:10.1029/2007GL032522.

Brown, L.L., Webber, J., Williams, M., Regan, S. & Seaman, S., 2013. Magnetism of the lower crust: observations from the Chipman Domain, Athabasca Granulite Terrain, northern Canada, *Tectonophysics,* **624–625,** 66–74.

Deng, J.F., Wu, Z.X., Zhao, G.C., Zhao, H.L., Luo, Z.H. & Mo, X.X., 1999. Precambrian granitic rocks, continental crustal evolution and craton formation of the North China Platform, *Acta Petrol. Sin.,* **15,** 190–198.

Doubrovine, P.V. & Tarduno, J.A., 2004. Self-reversed magnetization carried by titanomaghemite in oceanic basalts, *Earth planet. Sci. Lett.,* **222,** 959–969.

Doubrovine, P.V. & Tarduno, J.A., 2006. Geomagnetism and Paleomagnetism/Marine Geology and Geophysics Alteration and self-reversal in oceanic basalts, *J. geophys. Res.,* **111,** doi:10.1029/2006JB004468.

Dunlop, D.J., 2002. Theory and application of the Day plot (Mrs/Ms versus Hcr/Hc): 2. Application to data for rocks, sediments, and soils, *J. geophys. Res*., **107,** 2057, doi:10.1029/2001JB000487.

Dunlop, D.J., Özdemir, Ö. & Rancourt, D.G., 2006. Magnetism of biotite crystals, *Earth planet. Sci. Lett.,* **243,** 805–819.

Dunlop, D.J., Özdemir, Ö. & Costanzo-Alvarez, V., 2010. Magnetic properties of rocks of the Kapuskasing uplift (Ontario, Canada) and origin of long-wavelength magnetic anomalies, *Geophys. J. Int.,* **183,** 645–658.

Ferré, E.C., Friedman, S.A., Martín-Hernández, F., Feinberg, J.M., Conder, J.A. & Ionov, D.A., 2013. The magnetism of mantle xenoliths and potential implications for sub-Moho magnetic sources, *Geophys. Res. Lett.,* **40,** 105–110.

Ferré, E.C., Friedman, S.A., Martín-Hernández, F., Feinberg, J.M., Till, J.L., Ionov, D.A. & Conder, J.A., 2014. Eight good reasons why the uppermost mantle could be magnetic, *Tectonophysics,* **624–625,** 3–14.

Frost, B.R., 1991. Magnetic petrology: factors that control the occurrence of magnetite in crustal rocks, *Rev. Miner.,* **25,** 489–509.

Frost, B.R. & Lindsley, D.H., 1992. Equilibria among Fe-Ti oxides, pyroxene, olivine, and quartz: part II. Application, *Am. Mineral.,* **77,** 1004–1020.

Frost, B.R. & Shive, P.N., 1986. Magnetic mineralogy of the lower continental crust, *J. geophys. Res*., **91,** 6513–6521.

Kletetschka, G. & Stout, J.H., 1998. The origin of magnetic anomalies in lower crustal rocks, Labrador, *Geophys. Res. Lett.,* **25,** 199–202.

Langel, R.A. & Hinze, W.J., 1998. *The Magnetic Field of the Earth's Lithosphere,* Cambridge Univ. Press.

Lindsley, D.H. & Frost, B.R., 1992. Equilibria among Fe-Ti oxides, pyroxene, olivine, and quartz: part I. Theory, *Am. Mineral.,* **77,** 987–1003.

Liu, Q.S., 2011. Why are Q-ratios high in the Sulu UHP metamorphic rocks?, *J. Earth Sci.,* **22,** 115–116.

Liu, Q.S., Gao, S. & Xu, Q.D., 1994. Magnetic structure of the Dengfeng-Lushan crustal cross-section, Henan, *Sci. China (Series B),* **37,** 911–1000.

Liu, Q.S., Gao, S. & Liu, Y.S., 2000. Magnetic structure of the continental crust as revealed by the Wutai-Jijing crustal cross-section in the North China craton, *J. Geodyn.,* **29,** 1–13.

Liu, Q.S., Liu, Q.S., Zhang, Z.M., Xu, H.J., Chan, L.S., Yang, T. & Jin, Z.M., 2007. Magnetic properties of ultrahigh-pressure eclogites controlled by retrograde metamorphism: a case study from the ZK 703 drillhole in Donghai, eastern China, *Phys. Earth planet. Inter.,* **160,** 181–191.

Liu, Q.S., Liu, Q.S., Liu, Y.S., Gao, S., Yang, T., Luo, Y.H. & Jin, Z.M., 2008. Magnetic study of mafic granulite xenoliths from the Hannuoba basalt, North China, *Geochem. Geophys. Geosyst.,* **21,** Q06008, doi:10.1029/2008GC001952.

Liu, Q.S. *et al.*, 2009. Magnetic study of the UHP eclogites from the Chinese Continental Scientific Drilling (CCSD) Project, *J. geophys. Res.,* **114,** B02106, doi:10.1029/2008JB005917.

Liu, Q.S., Zeng, Q.L., Zheng, J.P., Yang, T., Qiu, N., Liu, Z.F., Luo, Y.H. & Jin, Z.M., 2010. Magnetic properties of serpentinized garnet peridotites from the CCSD main hole in the Sulu ultrahigh-pressure metamorphic belt, eastern China, *J. geophys. Res.,* **115,** B06104, doi:10.1029/2009JB000814.

Liu, Q.S., Frost, B.R., Wang, H.C., Zheng, J.P., Zeng, Q.L. & Jin, Z.M., 2012. Magnetic petrology of high Fe-Ti eclogites from the CCSD main hole: implications for subduction-zone magnetism, *J. geophys. Res.,* **117,** B07102, doi:10.1029/2011JB008621.

Liu, Q.S., Wang, H.C., Zheng, J.P., Zeng, Q.L. & Liu, Q.S., 2013. Petromagnetism properties of granulite-facies rocks from the northern North China craton: implications for magnetic and evolution of the continental lower crust, *J. Earth Sci.,* **24,** 12–28.

Liu, Q.S., Qiu, N., Zheng, J.P., Li, Z.Y. & Wang, H.C., 2015. Crustal large-scale serpentinized mantle peridotite body in the Sulu ultrahigh-pressure metamorphic belt, eastern China: evidence from gravity and magnetic anomalies, *J. Struct. Geol.,* **70,** 190–199.

McEnroe, S.A., Langenhorst, F., Robinson, P., Bromiley, G.D. & Shaw, C.S.J., 2004. What is magnetic in the lower crust? *Earth planet. Sci. Lett.,* **226,** 175–192.

Olesen, O., Henkel, H., Kaada, K. & Tveten, E., 1991. Petrophysical properties of a prograde amphibolite-granulite facies transition zone at Sigerfjord, Vesterålen, northern Norway, *Tectonophysics,* **192,** 33–39.

Oufi, O., Cannat, M. & Horen, H., 2002. Magnetic properties of variable serpentinized abyssal peridotite, *J. geophys. Res.,* **107**(B5), 2095, doi:10.1029/2001JB000549.

Peters, C. & Dekkers, M.J., 2003. Selected room temperature magnetic parameters as a function of mineralogy, concentration and grain size, *Phys. Chem. Earth,* **28,** 659–694.

Pilkington, M. & Percival, J.A., 1999. Crustal magnetization and long-wavelength aeromagnetic anomalies of the Minto block, Quebec, *J. geophys. Res.,* **104,** 7513–7526.

Piper, J.D.A. & Zhang, J.S., 1999. Palaeomagnetism, rock magnetism and magnetic fabrics in Precambrian metamorphic terranes of the Huabei Shield, North China, *J. Asian Earth Sci.,* **17,** 395–419.

Piper, J.D.A., Mallik, S.B., Bandyopadhyay, G., Mondal, S. & Das, A.K., 2003. Palaeomagnetic and rock magnetic study of a deeply exposed continental section in the Charnockite Belt of southern India: implications to crustal magnetization and palaeoproterozoic continental nuclei, *Precambrian Res.,* **121,** 185–219.

Piper, J.D.A., Zhang, J.S., Huang, B.C. & Roberts, A.P., 2011. Palaeomagnetism of Precambrian dyke swarms in the North China Shield: the $\sim$1.8 Ga LIP event and crustal consolidation in late Palaeoproterozoic times, *J. Asian Earth Sci.,* **41,** 504–524.

Ramachandran, C., 1990. Metamorphism and magnetic susceptibilities in South Indian granulite terrain, *J. Geol. Soc. India,* **35,** 395–403.

Ravat, D.N., Whale, K.A., Pilkington, M., Sabaka, T. & Purucker, M., 2002. Compatibility of high-altitude aeromagnetic and satellite-altitude magnetic anomalies over Canada, *Geophysics,* **67,** 546–554.

Renne, P.R., Scott, G.R., Glen, J.M.G. & Feinberg, J.M., 2002. Oriented inclusions of magnetite in clinopyroxene: source of stable remanet magnetization in gabbros of the Messum Complx, Namibia, *Geochem. Geophys. Geosyst.,* **31,** 1079, doi:10.1029/2002GC000319.

Schlinger, C.M., 1985. Magnetization of lower crust and interpretation of regional magnetic anomalies: example from Lofoten and Vesterålen, Norway, *J. geophys. Res.,* **90,** 11 484–11 504.

Schlinger, C.M., Khan, M.J. & Wasilewski, P., 1989. Rock magnetism of the Kohistan island arc, Pakistan, *Geol. Bull. Univ. Peshawar,* **22,** 83–101.

Shive, P.N. & Fountain, D.M., 1988. Magnetic mineralogy in an Archean crustal cross section: implications for crustal magnetization, *J. geophys. Res.,* **93,** 12 177–12 186.

Shive, P.N., Blakely, R.J., Frost, B.R. & Fountain, D.M., 1992. Magnetic properties of the lower continental crust, in *Continental Lower Crust,* pp. 145–178, eds Fountain, D.M., Arculus, R. & Kay, R.W., Elsevier.

Tarling, D.H., 1983. *Palaeomagnetism: Principles and Applications in Geology, Geophysics, and Archaeology,* Chapman and Hall Ltd.

Toft, P.B., Arkani-Hamed, J. & Haggerty, S.E., 1990. The effect of serpentinization on density and magnetic sueceptibility: a petrophysical model, *Phys. Earth planet. Inter.,* **65,** 137–157.

Toft, P.B., Scowen, P.A.H., Arkni-Hamed, J. & Francis, D., 1993. Demagnetization by hydration in deep-crustal rocks in the Grenville province of Quebec, Canada: implications for magnetic anomalies of continental collision zones, *Geology,* **21,** 999–1002.

Wasilewski, P. & Fountain, D.M., 1982. The Ivrea Zone as a model for the distribution of magnetization in the continental crust, *Geophys. Res. Lett.,* **9,** 333–336.

Wasilewski, P.J. & Mayhew, M.A., 1982. Crustal xenoliths magnetic properties and long wavelength anomaly source requirements, *Geophys. Res. Lett.,* **9,** 329–332.

Wasilewski, P.J. & Warner, R.D., 1988. Magnetic petrology of deep crustal rocks-Ivrea Zone, Italy, *Earth planet. Sci. Lett.,* **87,** 347–361.

Williams, M.C., Shive, P.N., Fountain, D.M. & Frost, B.R., 1985. Magnetic properties of exposed deep crustal rocks from the Superior Province of Manitoba, *Earth planet. Sci. Lett.,* **76,** 176–184.

Xu, H.J., Jin, Z.M., Mason, R. & Ou, X.J., 2009. Magnetic susceptibility of ultrahigh-pressure eclogite: the role of retrogression, *Tectonophysics,* **475,** 279–290.

Zhang, R.Y. & Cong, B.L., 1982. Mineralogy and P-T conditions of crystallization of Early Archaean granulites from Qianxi County, NE China, *Sci. Sin. (Series B),* **26,** 96–112.

Zhang, J.S. & Piper, J.D.A., 1994. Magnetic fabric and post-orogenic uplift and cooling magnetisations in a Precambrian granulite terrain: the Datong-Huai'an region of the North China Shield, *Tectonophysics,* **234,** 227–246.

Zhang, J. S., Lao, Q.Y. & Li, Y., 1999. Tectonic implication of aeromagnetic anomaly and evolution of Huabei-South Tarim-Yangtze superlandmass, *Earth Sci. Front.,* **6,** 379–390 (in Chinese with English abstract).